S21C-0453

AGU 100 FALL MEETING
Washington, D.C. | 10–14 Dec 2018

Mechanism of microearthquakes from acoustic emission in a laboratory: How to evaluate efficiently a large amount of data

Jan Šílený[1], Zuzana Jechumtálová[1] and Matěj Petružálek[2]

1) Institute of Geophysics, Czech Academy of Sciences; 2) Institute of Geology, Czech Academy of Sciences

INSTITUTE OF GEOPHYSICS OF THE CZECH ACADEMY OF SCIENCES

INSTITUTE OF GEOLOGY OF THE CZECH ACADEMY OF SCIENCES

MOTIVATION

Employing of a constrained source model to enhance robustness of the inverse task

Traditional source model: full moment tensor (MT)

- describes both shear and non-shear (tensile/collapsing) sources ⇨ suitable for tectonic and induced events
- in poorly constrained inverse tasks (inexact velocity model, mislocation, poor geometry of observation) may be resolved poorly (especially the DC vs. non-DC contents)

➡ constrained source model is often useful in practice

Traditional constraint in earthquake seismology - deviatoric MT is not capable to describe a volume change ⇨ not useful in induced seismicity

The clue:
Shear-Tensile Crack source model

SHEAR-TENSILE CRACK SOURCE MODEL

Shear-Tensile Crack (STC): combination of a shear slip and opening/closing the fault

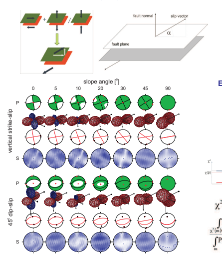

full MT: 6 parameters

STC: 5 parameters
dip, strike, rake of the shear slip
slope angle (slip vector off the fault)
scalar moment

Error analysis of resolved STC: confidence regions

small confidence region ⇨ well determined solution
large confidence region ⇨ poorly constrained solution

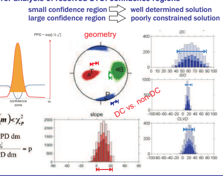

$$\chi^2(m) < \chi^2_p$$

$$\frac{\int_{\chi^2(m)<\chi^2_p} PPD\, dm}{\int_m PPD\, dm} = p$$

STATISTICS OF FRACTURING DURING LOADING

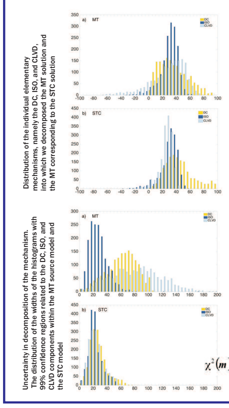

Distribution of the individual elementary mechanisms, namely the DC, ISO, and CLVD, into which we decomposed the MT solution and the MT corresponding to the STC solution

Uncertainty in decomposition of the mechanism. The distribution of the widths of the histograms with 99% confidence regions related to the DC, ISO, and CLVD components within the MT source model and the STC model

A set of 1,630 reliably retrieved AE source mechanisms were analyzed in detail.

- due to the direct influence of contact conditions, all AE events localized within the vicinity (1 cm) of the loading platens were rejected from a representative data set
- the solution of the STC inversion with good misfit (NRMS < 0.5) was used only

The set consisted of - 731 tensional AE events
694 combined AE events
205 shear AE events

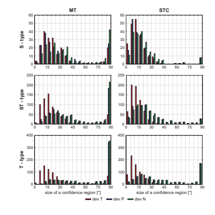

Uncertainty in the orientation of the mechanism as determined in the MT (left) and the STC (right) approach. The distribution in [size] of the confidence regions of T are provided in red, P in [blue] and N in green for AEs recorded during the loading experiment. The events are sorted into shear – S (top), shear-tensile – ST (middle), and tensile – T (bottom) types.

EXEMPLARY AE SOURCE TYPES

Examples of the three types of mechanisms selected from the series recorded during the loading experiment

- event No. 3,043 is a S-type (shear-type mechanism)
- event No. 3,289 is a ST-type (shear-tensile mechanism)
- event No. 7,001 is a T-type (tensile mechanism)

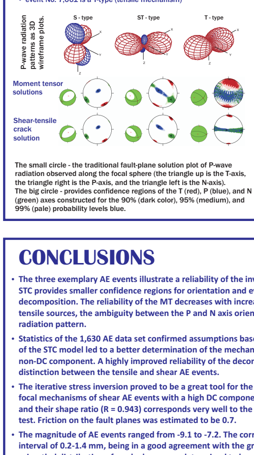

The small circle - the traditional fault-plane solution plot of P-wave radiation observed along the focal sphere (the triangle up is the T-axis, the triangle right is the P-axis, and the triangle left is the N-axis). The big circle - provides confidence regions of the T (red), P (blue), and N (green) axes constructed for the 90% (dark color), 95% (medium), and 99% (pale) probability levels blue.

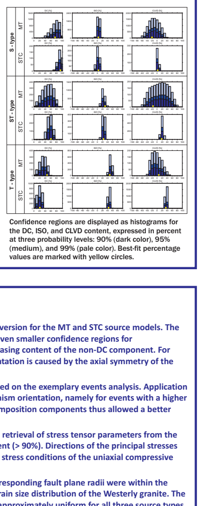

Confidence regions are displayed as histograms for the DC, ISO, and CLVD content, expressed in percent at three probability levels: 90% (dark color), 95% (medium), and 99% (pale color). Best-fit percentage values are marked with yellow circles.

CONCLUSIONS

- The three exemplary AE events illustrate a reliability of the inversion for the MT and STC source models. The STC provides smaller confidence regions for orientation and even smaller confidence regions for decomposition. The reliability of the MT decreases with increasing content of the non-DC component. For tensile sources, the ambiguity between the P and N axis orientation is caused by the axial symmetry of the radiation pattern.
- Statistics of the 1,630 AE data set confirmed assumptions based on the exemplary events analysis. Application of the STC model led to a better determination of the mechanism orientation, namely for events with a higher non-DC component. A highly improved reliability of the decomposition components thus allowed a better distinction between the tensile and shear AE events.
- The iterative stress inversion proved to be a great tool for the retrieval of stress tensor parameters from the focal mechanisms of shear AE events with a high DC component (> 90%). Directions of the principal stresses and their shape ratio (R = 0.943) corresponds very well to the stress conditions of the uniaxial compressive test. Friction on the fault planes was estimated to be 0.7.
- The magnitude of AE events ranged from -9.1 to -7.2. The corresponding fault plane radii were within the interval of 0.2-1.4 mm, being in a good agreement with the grain size distribution of the Westerly granite. The azimuthal distribution of crack planes was determined to be approximately uniform for all three source types. The angle, α, between the loading direction and the crack plane increased with increasing DC component. Average values for the three particular source types were: 16°, 21°, and 26°, for the tensile, shear-tensile and shear AEs, respectively.
- Source types with a high non-DC component (T = 46%, ST = 42%) dominated in both the stable and unstable microcracking region, while shearing (12%) remained in the minority. Microcracking mainly occurred within the middle circumferential portion of the specimen, while the AE activity missed within the upper and bottom conical portions of specimen. Flaking at middle-height, the region of high AE activity, lead to failure of the specimen. Both the AE locations and the manner of failure indicate a perfect confinement end-boundary conditions between the tested specimen and the loading platens.

ROCK MATERIAL AND THE EXPERIMENTAL SETUP

Due to its small grain size, homogeneity, and low anisotropy, Westerly Granite (WG) was chosen as a convenient rock material.

For our experiment, the original cylindrical specimen (height 104 mm, diameter 52 mm) was ground into the shape of an almost regular octagonal prism.

Using the MTS system, model 815, the specimen was uniaxially loaded in the compression up to peak stress. Loading was controlled with a linear combination of axial stress (σ) and axial strain (ε).

Twelve of the sensors were directly attached to the surface of the specimen and two were embedded in the top and bottom loading platens.

The apparatus was set up in a triggered regime (38 dB).

The sampling rate was 10 MHz.

Approximately 21,000 AE events were registered.

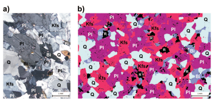

a) Westerly Granite (WG) - a microphotograph of a thin section: Q-quartz, Pl-plagioclase, Kfs-K feldspar, Bi-biotite; b) mineral composition obtained from the TIMA analysis, where R stands for grains other than the four rock forming minerals.

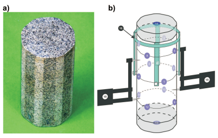

a) The Westerly Granite (WG) prismatic specimen prior to testing. b) The experimental setup: 1-14 – the AE/US sensors, Fuji AE204A; 15 – the extensometers, MTS 632.11D-90; and 16 - the cantilever, Ergotech.

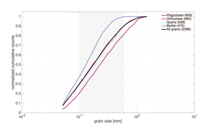

Westerly Granite (WG) – grain size distribution.

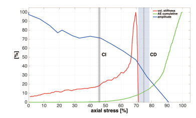

a) Estimations of crack initiation and the crack damage thresholds. The red color is volumetric stiffness, the green color is the acoustic emission activity, and the blue color is the first arrival amplitude. All of the quantities were normalized. CI – crack initiation stress, CD – crack damage stress.

THE STC MECHANISM IN A ROCK MECHANICS CONTEXT

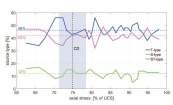

Source type distribution. The blue color indicates tension type, the green color indicates shear type and the magenta color indicates combined type, shaded area corresponds to crack damage stress

The moment magnitude Mw was calculated from the scalar seismic moment. Moment magnitudes for the AE data set were in the interval of -9.1 to -7.5. The magnitude distribution is rather independent of the source type, with a slight shift to higher values for shear cracks. To estimate the source radius, r, we used the Brune's formula. The radii of registered AE events were in the range of 0.2-1.4 mm, corresponding to the grain size distribution.

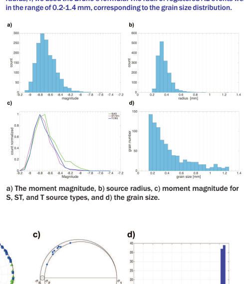

a) The moment magnitude, b) source radius, c) moment magnitude for S, ST, and T source types, and d) the grain size.

The iterative stress inversion (Vavryčuk 2014) was applied to calculate 4 parameters of the stress tensor: the directions of the principal stresses (σ_1, σ_2, and σ_3) and the shape ratio $R = (\sigma_1 - \sigma_2) / (\sigma_1 - \sigma_3)$. Since the inversion serves for the processing of earthquakes (having high DC), it is sensitive to the presence of a non-DC component. Therefore, the 17 best shear-type events (DC > 90%, NRMS < 0.3), located in the unstable microcracking range, served as input for the inversion.

The obtained results agreed very well with the stress condition of the uniaxial compression test.

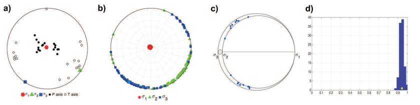

a) The orientation of the $_1$, σ_2, and σ_3 stress axes together with the P and T axes for the 17 selected AE source mechanisms.
b) The confidence zones for $_1$, σ_2, and σ_3 stress axes. c) Mohr's circle diagram with positions of the identified fault planes.
d) Confidence zones for the shape ratio, yellow circle – the best-fit value.

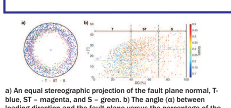

a) An equal stereographic projection of the fault plane normal, T-blue, ST – magenta, and S – green. b) The angle (α) between loading direction and the fault plane versus the percentage of the DC component.

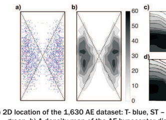

a) 2D location of the 1,630 AE dataset: T- blue, ST – magenta, and S – green. b) A density map of the AE hypocenter distribution. c) The measured crack density distribution for the perfect confinement end-boundary conditions, upper half of the specimen.
d) The idealized crack density distribution for the perfect confinement end-boundary conditions, upper half of the specimen.

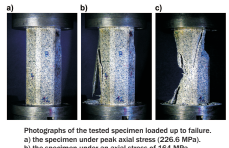

Photographs of the tested specimen loaded up to failure.
a) the specimen under peak axial stress (226.6 MPa).
b) the specimen under an axial stress of 164 MPa.
c) the specimen at the moment of failure (92 MPa).

Petružálek, M., Jechumtálová, Z., Kolář, P., Adamová, P., Svitek, T., Šílený, J. & Lokajíček, T., 2018. Acoustic Emission in a Laboratory: Mechanism of Microearthquakes Using Alternative Source Models. *J. Geophys. Res.*, 123, 4965-4982, doi:10.1029/2017JB015393.

Petružálek, M., Jechumtálová, Z., Šílený, J., Kolář, P., Svitek, T., Lokajíček, T., Turková, I., Kotrlý, M. & Onysko, R., 2018. Fracturing of Westerly Granite: Application of the Shear-Tensile Source Model to Acoustic Emissions, *Rock Mechanics and Rock Engineering*, submitted.